

Supporting Information

Anchoring ultrafine PtNi nanoparticles on N-doped graphene for highly efficient hydrogen evolution reaction

Jiehua Bao,^a Jiaqi Wang,^a Yuming Zhou,^{*a} Yingjie Hu,^b Zewu Zhang,^c Tongfei Li,^a Yi Xue,^a Chang Guo,^a and Yiwei Zhang ^{*a}

^a School of Chemistry and Chemical Engineering, Southeast University, Jiangsu Optoelectronic Functional Materials and Engineering Laboratory, Nanjing 211189, China.

^b School of Environmental Science, Nanjing Xiaozhuang University, Nanjing 211171, China.

^c School of Materials Science and Engineering, Nanjing Institute of Technology, Nanjing 211167, China.

Corresponding Authors

*E-mail (Y. M. Zhou): ymzhou@seu.edu.cn

Tel: +862552090617; Fax: +862552090617

*E-mail (Y. W. Zhang): zhangchem@seu.edu.cn

Material and methods

Materials

Graphite flake (C), sulfuric acid (H_2SO_4), phosphoric acid (H_3PO_4), potassium permanganate (KMnO_4), hydrogenperoxide (H_2O_2), hydrochloric acid (HCl), (3-Aminopropyl) triethoxysilane (APTES, $\text{C}_9\text{H}_{23}\text{NO}_3\text{Si}$), Chloroplatinic acid ($\text{H}_2\text{PtCl}_6 \cdot 6\text{H}_2\text{O}$), sodium chloride (NaCl), nickel chloride hexahydrate ($\text{NiCl}_2 \cdot 6\text{H}_2\text{O}$), cobalt chloride hexahydrate ($\text{CoCl}_2 \cdot 6\text{H}_2\text{O}$), sodium borohydride (NaBH_4), ammonia aqueous (NH_4OH), sodium hydroxide (NaOH), Nafion, commercial Pt/C (20%) were purchased from Sinopharm Chemical Reagent Co., Ltd. All chemicals were of analytical grade and used without further purification. De-ionized water was obtained by reversed osmosis followed by ion-exchange and filtration.

Synthesis of PtNi/rGO(N)

GO was synthesized according to a modified Hummers' method.^{25, 26} PtNi/rGO(N) was prepared via a chemical reduction method as follows: 1.4 mL APTES was put into 25.0 mL GO aqueous solution (2.0 mg mL^{-1}) little by little with sonicating. Then, NiCl_2 (0.02 M, 215 μL), H_2PtCl_6 (0.02M, 65 μL) and NaCl (0.08 mg) were added, and this mixture was kept with magnetic stirring for 3 h. Finally, 1.0 mL of 100.0 mM NaBH_4 was added into the above mixed solution with stirring. The PtNi/rGO(N) was washed and separated by centrifugation.

Synthesis of PtNi/N-rGO

Firstly, for preparation of N-rGO, 8.0 mL NH_4OH and 100.0 mg NaOH were added into GO aqueous solution; the mixed solution was transferred to a Teflon-lined autoclave for reaction at 200°C to get N-rGO. Thereafter, NiCl_2 (0.02 M, 215 μL), H_2PtCl_6 (0.02M, 65 μL), NaCl (0.08 mg) and H_2O (65 μL) were added, and this mixture was kept with magnetic stirring. Finally, NaBH_4 (100.0 mM, 1.0 mL) was added as the reducing agent to obtain the PtNi/N-rGO.

Synthesis of Pt/rGO(N), Ni/rGO(N), PtNi/rGO, 2PtNi/rGO(N) and PtCo/rGO(N)

For comparison, the Pt/rGO(N), Ni/rGO(N) and PtNi/rGO were prepared using the similar method without addition of NiCl_2 , H_2PtCl_6 and APTES, respectively, and the un-supported PtNi was synthesized

without addition of both APTES and GO. The 2PtNi/rGO(N) was prepared using the similar method, adding twice the NiCl₂ and H₂PtCl₆. The PtCo/rGO(N) was prepared using the similar method, replacing NiCl₂ with an equal amount of CoCl₂.

Characterization

The morphology and texture of the materials were observed using transmission electron microscopy (TEM, JEM-2010). The Brunauer-Emmett-Teller (BET) surface area analysis of the samples was performed using Micromeritics ASAP 2020 apparatus, which were determined by analyzing adsorption data in the relative pressure (p/p_0) range of 0.02-0.15. The crystal structures of the as-prepared catalysts were characterized using an X-ray diffractometer (XRD) with Cu K α radiation ($\lambda = 1.5418 \text{ \AA}$) operating at 40 kV and 40 mA. The chemical bonds in the samples were measured using Fourier transform infrared spectra (FT-IR, BRUKER VECTOR-22). Raman spectrum was collected using a laser Raman spectrometer (Thermo Fisher) with a laser of 532 nm wavelength. X-ray photoelectron spectroscopy (XPS) was carried out on an ESCALAB MKII X-ray photo-electron spectrometer equipped with an Mg K α . UV-vis diffuse reflectance spectroscopy of the samples was performed on a UV-vis spectrophotometer (Shimadzu UV-3600). The metal loading of the catalysts was determined by inductively coupled-plasma atomic emission spectroscopy (ICP-AES) using a Thermo iCAP 6300 spectrometer.

Electrochemical measurements

Electrochemical properties of the samples were evaluated in a three-electrode system with an electrochemical workstation (CH Instruments 660E, Shanghai Chenhua) at 298K. The glassy carbon disk (GCE 4.0 mm in diameter), coated by catalysts films, graphite rod and Ag/AgCl electrode were used as the working electrode, counter electrode and reference electrode, respectively. For the preparation of the catalyst films, 5.0 mg of catalyst was dispersed in 1.0 mL solution containing 30.0 μL of 5 wt% Nafion solution and 970.0 μL of ethanol. Then 10.0 μL the mixture after 30 min of ultrasound treatment was dropped on the electrode by using a micropipette, and then dried in air. The electrolyte of electrochemical

tests was 0.5 M H₂SO₄ solution. All potentials are referred to the RHE. Firstly, the linear sweep voltammetry (LSV) curves were carried out at a scan rate of 10 mV s⁻¹. The catalyst was cycled numerous times by CV until a stable CV curve was obtained before testing. The Tafel plots were obtained from LSV curves with a scan rate of 1 mV s⁻¹. The electrochemical impedance spectroscopy (EIS) was performed in a frequency range from 100 kHz to 0.01 Hz. The stability tests were carried out by repeating the potential scan at a sweep rate of 100 mV s⁻¹ with 1,000 CV cycles, and the chronoamperometry curves were obtained by holding the potential at -150 mV. All these results were obtained by iR-compensation.

All the potentials were determined with respect to RHE using the equation:

$$E_{\text{RHE}} = E_{\text{SCE}} + 0.241 \text{ V} + 0.0591 \text{ pH}$$

The Tafel slopes were calculated by fitting to the Tafel equation:

$$\eta = b \log j + c$$

where b is the Tafel slope, j is the current density and c is the intercept relative to j_0 . The exchange current density (j_0) is calculated by extrapolating the Tafel plots to X-axis according to Tafel equation.

ECSA evaluation

The ECSA was estimated from the electrochemical double-layer capacitance of the hybrids. The electrochemical double-layer capacitance was determined from the CV curves measured in the potential range of 0.15 to 0.3 V versus RHE according to the following equation:

$$C_{\text{dl}} = I_c / \nu$$

where C_{dl} , I_c , and ν are the double-layer capacitance (in farads per μg_{Pt}) of the electroactive materials, charging current (in milliamperes per μg_{Pt}), and scan rate (in millivolts per second), respectively. I_c was taken at the potential of 0.225 V versus RHE.

TOF calculation

TOF of the catalysts were calculated according to the following equations:

$$\text{TOF} = I / (2F \cdot n)$$

where I is the current (in amperes), F is the Faraday constant ($96,485.3 \text{ C mol}^{-1}$), and n is the number of moles of the active catalyst.

Supplementary figures

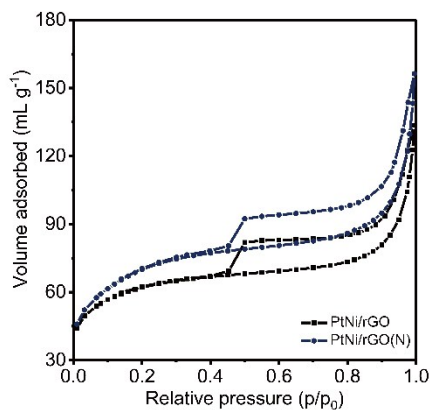


Fig. S1. Nitrogen adsorption–desorption isotherms of PtNi/rGO(N) and PtNi/rGO.

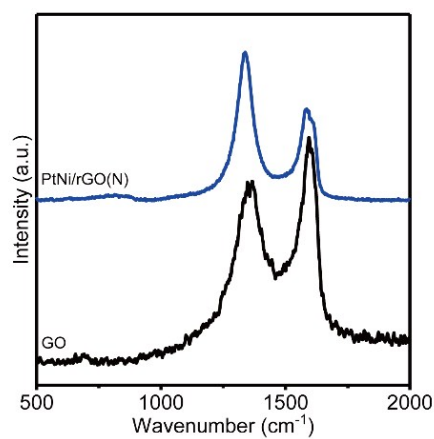


Fig. S2. Raman spectra of GO and PtNi/rGO(N).

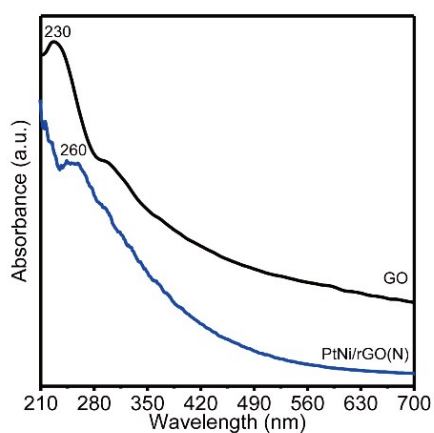


Fig. S3. UV-Vis absorption spectra of GO and PtNi/rGO(N).

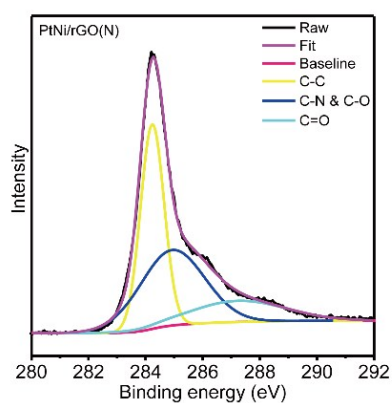


Fig. S4. High-resolution XPS spectra of C 1s in PtNi/rGO(N).

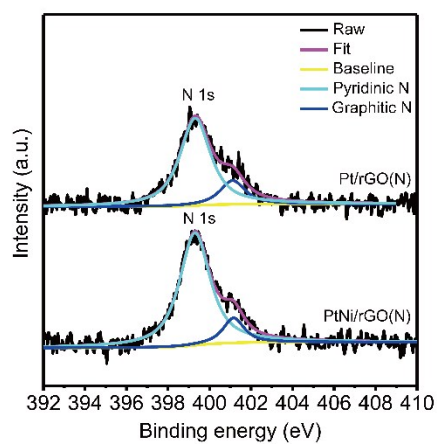


Fig. S5. High-resolution XPS spectra of N 1s for PtNi/rGO(N) and Pt/rGO(N).

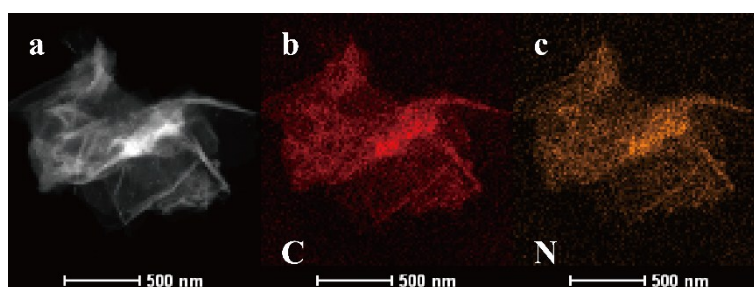


Fig. S6. (a) STEM images of the PtNi/rGO(N). EDX elemental mapping images of (b) C and (c) N.

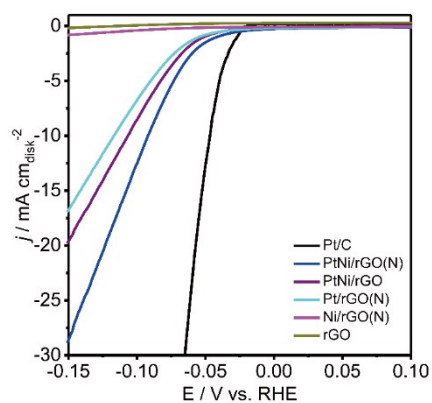


Fig. S7. HER polarization curves of the PtNi/rGO(N), Pt/rGO(N), Ni/rGO(N), rGO and the commercial Pt/C, after iR correction, in 0.5 M H₂SO₄ at 298K, normalized by the geometric area of the working electrode (disk).

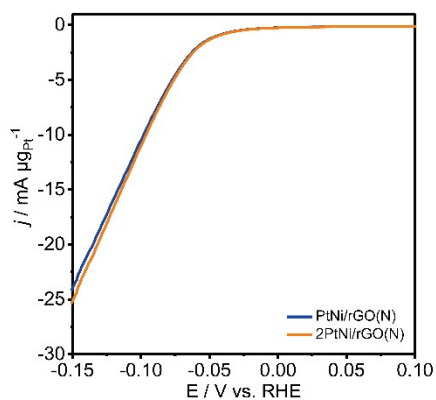


Fig. S8. HER polarization curves of the PtNi/rGO(N) and 2PtNi/rGO(N), after iR correction, in 0.5 M H₂SO₄, normalized by the mass of Pt.

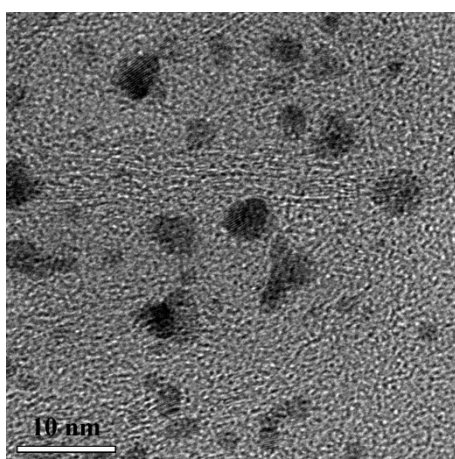


Fig. S9. TEM image of the 2PtNi/rGO(N).

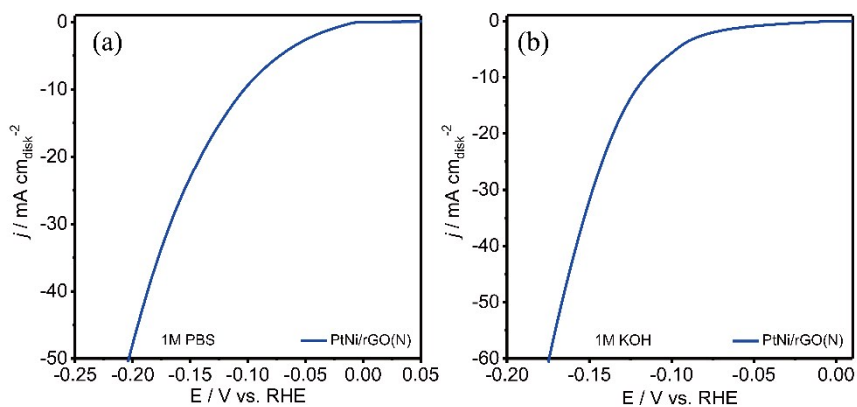


Fig. S10. HER polarization curves of the PtNi/rGO(N) in 1 M PBS (a) and KOH (b), normalized by the geometric area of the working electrode (disk), after iR correction.

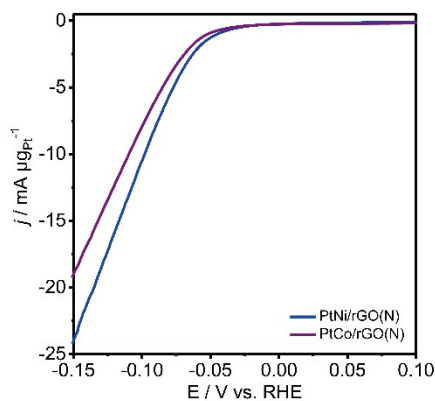


Fig. S11. HER polarization curves of the PtNi/rGO(N) and PtCo/rGO(N), after iR correction, in 0.5 M H₂SO₄, normalized by the mass of Pt

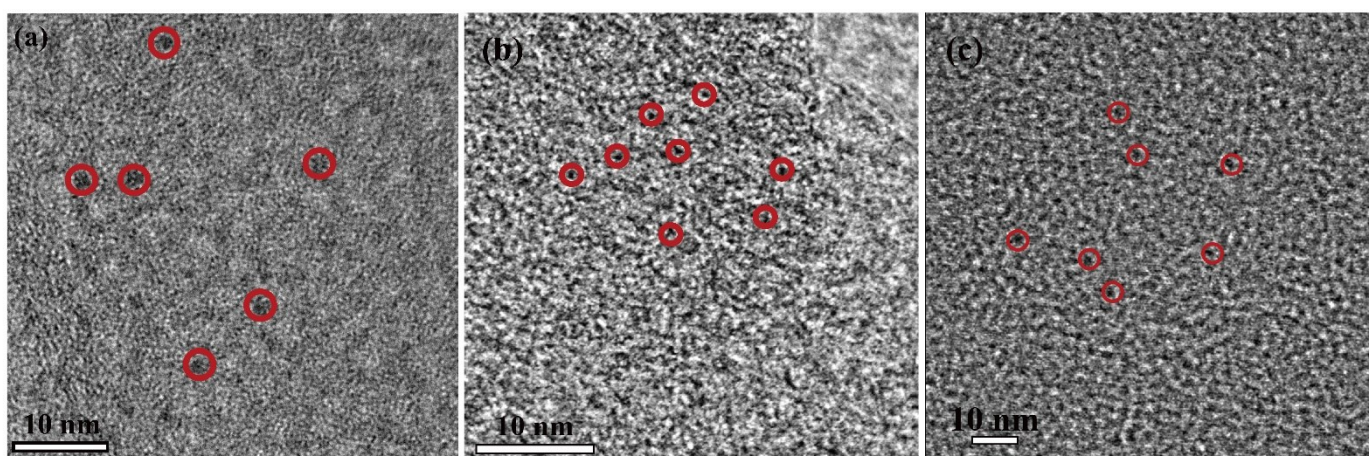


Fig. S12. TEM images of (a) before, (b) after 1,000 cycles and (c) after 20 h long-term stability test of the PtNi/rGO(N).

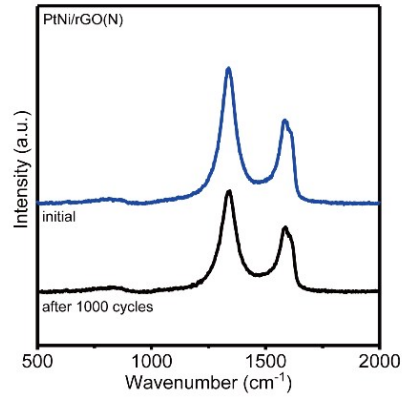


Fig. S13. Raman spectra of before and after 1,000 cycles of the PtNi/rGO(N).

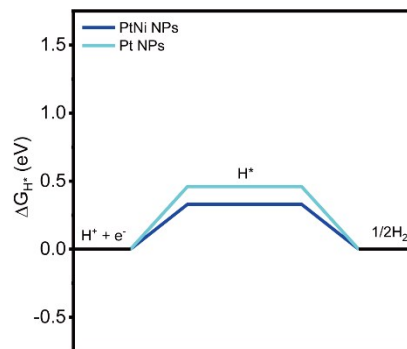


Fig. S14. Gibbs free energies (ΔG_{H^+}) on PtNi NPs and Pt NPs in acid environment.

Supplementary table

Table S1. Key parameters of PtNi/rGO(N) and PtNi/rGO.

	PtNi/rGO(N)	PtNi/rGO
S_{BET} ($\text{m}^2 \text{g}^{-1}$)	279.8	223.9
Pt content (wt%)	0.3	0.32
Ni content (wt%)	0.2	0.21
Overpotential at 10 mA $\mu\text{g}_{\text{pt}}^{-1}$ (mV)	98	116
Tafel slope (mV dec^{-1})	42.7	45.5
TOF at -150 mV (s^{-1})	24.3	16.6

Table S2. Comparison of the HER activity of PtNi/rGO(N) and other high-performance HER catalysts.

Catalyst	Electrolyte	Overpotential at 10 mA cm^{-2} (mV)	Tafel slope (mV dec^{-1})	Ref.
PtNi/rGO(N)	0.5 M H_2SO_4	92	42.7	This work
Pt/rGO(N)	0.5 M H_2SO_4	116	48.6	This work
PdNi-S	0.5 M H_2SO_4	103	80	S1
Pt-MoS ₂	0.5 M H_2SO_4	60	96	S2
Ni ₂ P/MoS ₂	0.5 M H_2SO_4	92	87.69	S3
WS ₂ /P, N, O-graphene	0.5 M H_2SO_4	125	52.7	S4
NiSe fiber	0.5 M H_2SO_4	230	64	S5
MoSe ₂ /N-graphene	0.5 M H_2SO_4	106	57	S6
MoS ₂ /graphene/Ni foams	0.5 M H_2SO_4	141	42.8	S7
Mo ₂ C/CNT	0.5 M H_2SO_4	152	55.2	S8
[Mo ₃ S ₁₃] ²⁻ /Graphene	0.5 M H_2SO_4	180	40	S9
PCP/NRGO	0.5 M H_2SO_4	229	127	S10

References

- S1. X. Yang, W. Xu, S. Cao, S. Zhu, Y. Liang, Z. Cui, X. Yang, Z. Li, S. Wu, A. Inoue and L. Chen, *Appl. Catal., B*, 2019, **246**, 156-165.
- S2. J. Deng, H. Li, J. Xiao, Y. Tu, D. Deng, H. Yang, H. Tian, J. Li, P. Ren and X. Bao, *Energy & Environmental Science*, 2015, **8**, 1594-1601.
- S3. M. Kim, M. A. R. Anjum, M. Lee, B. J. Lee and J. S. Lee, *Adv. Funct. Mater.*, 2019, **29**, 1809151.
- S4. J. Duan, S. Chen, B. A. Chambers, G. G. Andersson and S. Z. Qiao, *Adv. Mater.*, 2015, **27**, 4234-4241.
- S5. M.-R. Gao, Z.-Y. Lin, T.-T. Zhuang, J. Jiang, Y.-F. Xu, Y.-R. Zheng and S.-H. Yu, *J. Mater. Chem.*, 2012, **22**, 13662-13668.
- S6. M. Zhuang, Y. Ding, X. Ou and Z. Luo, *Nanoscale*, 2017, **9**, 4652-4659.
- S7. Y.-H. Chang, C.-T. Lin, T.-Y. Chen, C.-L. Hsu, Y.-H. Lee, W. Zhang, K.-H. Wei and L.-J. Li, *Adv. Mater.*, 2013, **25**, 756-760.
- S8. W. F. Chen, C. H. Wang, K. Sasaki, N. Marinkovic, W. Xu, J. T. Muckerman, Y. Zhu and R. R. Adzic, *Energy & Environmental Science*, 2013, **6**, 943-951.
- S9. J. Kibsgaard, T. F. Jaramillo and F. Besenbacher, *Nat. Chem.*, 2014, **6**, 248.
- S10. Y. Hou, Z. Wen, S. Cui, S. Ci, S. Mao and J. Chen, *Adv. Funct. Mater.*, 2015, **25**, 872-882.